Characterization of Two Distinct β_2-Microglobulin Unfolding Intermediates that May Lead to Amyloid Fibrils of Different Morphology†

Roger S. Armen‡,§ and Valerie Daggett*,‡,||

Biomolecular Structure and Design Program, University of Washington, Seattle, Washington 98195-7610, and Department of Medicinal Chemistry, University of Washington, Seattle, Washington 98195-7610

Received April 20, 2005; Revised Manuscript Received August 24, 2005

ABSTRACT: The self-assembly of β_2-microglobulin into fibrils leads to dialysis-related amyloidosis. pH-mediated partial unfolding is required for the formation of the amyloidogenic intermediate that then self-assembles into amyloid fibrils. Two partially folded intermediates of β_2-microglobulin have been identified experimentally and linked to the formation of fibrils of distinct morphology, yet it remains difficult to characterize these partially unfolded states at high resolution using experimental approaches. Consequently, we have performed molecular dynamics simulations at neutral and low pH to determine the structures of these partially unfolded amyloidogenic intermediates. In the low-pH simulations, we observed the formation of α-sheet structure, which was first proposed by Pauling and Corey. Multiple simulations were performed, and two distinct intermediate state ensembles were identified that may account for the different fibril morphologies. The predominant early unfolding intermediate was nativelike in structure, in agreement with previous NMR studies. The late unfolding intermediate was significantly disordered, but it maintained an extended elongated structure, with hydrophobic clusters and residual α-extended chain strands in specific regions of the sequence that map to amyloidogenic peptides. We propose that the formation of α-sheet facilitates self-assembly into partially unfolded prefibrillar amyloidogenic intermediates.

β_2-Microglobulin (β_2m)[1] is a noncovalently bound light chain of the human class I major histocompatibility complex (MHC-1) (*1*). Cells displaying MHC-1 on their cell surface regularly release β_2m during the process of turnover (*2*). β_2m is then transported to the kidneys where it is normally filtered and degraded after reabsorption in the proximal tubules (*3*). Patients with kidney dysfunction have a reduced ability to filter β_2m from the plasma and consequently exhibit an up to 60-fold increase in the circulating level of β_2m (*2*, *3*). During the process of hemodialysis, high levels of β_2m are released from blood cells that are brought into contact with the hemodialysis membrane, which also contributes to the increased level of β_2m (*4*−*6*). Increased β_2m serum levels have been linked to pathogenic amyloid formation in the musculoskeletal system (*2*). Large amounts of β_2m amyloid deposits are found in the joints, which can lead to a variety of arthropathies (*2*). Taken collectively, pathogenic β_2m amyloid formation in kidney disease patients is called dialysis-related amyloidosis, and it is a severe complication for patients on long-term hemodialysis (*2*, *3*).

High concentrations of β_2m alone are insufficient for amyloid formation (*7*, *8*). Instead, unfolding of the protein into a partially structured conformation is required for the formation of aggregates and fibrils (*3*, *9*). Several triggers of partial unfolding have been suggested to occur in vivo, including increased local concentrations of copper in the proximity of dialysis membranes (*8*). An increased copper concentration can lead to this partially unfolded state under physiological conditions at neutral pH (*8*, *10*, *11*), although copper is not necessary for the formation of fibrils in vitro, or the stabilization of the fibrils (*12*).

The folding of β_2m has been studied with biophysical methods, including fluorescence spectroscopy, far- and near-UV circular dichroism, 8-anilino-1-naphthalenesulfonic acid binding, nuclear magnetic resonance (NMR) spectroscopy, hydrogen exchange, and double-jump assays (*13*, *14*). These studies suggest that β_2m folds and unfolds in a sequential manner populating two distinct intermediates, I_1 and I_2 (*13*, *14*).[2] The hypothesis is that the intermediates monitored during folding correspond to the unfolding intermediates linked to amyloidosis. The first unfolding intermediate, I_1, is nativelike, with a large amount of secondary structure and some nonnative tertiary structure, while the later unfolding intermediate, I_2, is substantially disordered but retains a large amount of secondary structure. The I_1 intermediate has an equilibrium population of approximately 15% at physiologi-

† Partial support for this work was provided by the National Institutes of Health (Grant GM 50789 to V.D.). R.S.A. was supported by an NIH Molecular Biophysics Training Grant (National Research Service Award 5 T32 GM 08268).

* To whom correspondence should be addressed. E-mail: daggett@u.washington.edu. Phone: (206) 685-7420. Fax: (206) 685-3252.

‡ Biomolecular Structure and Design Program.

§ Current address: The Scripps Research Institute, 10666 N. Torrey Pines Rd., La Jolla, CA 92037.

|| Department of Medicinal Chemistry.

[1] Abbreviations: β_2m, β_2-microglobulin; MD, molecular dynamics; rmsd, root-mean-square deviation.

[2] Given that it is the unfolding intermediates that are linked to amyloidosis and we are directly monitoring unfolding by MD, we number the intermediates in the unfolding direction. For example, I_1 is the first, which corresponds to the second intermediate in the folding direction.

10.1021/bi050731h CCC: $30.25
Published on Web 11/16/2005

cal pH and temperature (*9*).

β_2m forms fibrils of two distinct morphologies that have been specifically linked to the two unfolding intermediates (*15*). Short and curved fibrils form rapidly in a pH range of 3−5, and long and straight fibrils form in a pH range of 1.5−3 in salt (*15*, *16*). The curved fibrils are derived from the nativelike intermediate I_1, which is the dominant conformation at pH 4 (*15*), and the linear fibrils form slowly from the more disordered intermediate, I_2, which is the dominant conformation at pH 1.6 (*15*, *17*). The I_2 intermediate is significantly more unfolded and may be a highly populated conformation in the denatured state (*13*). The I_2 intermediate is less amyloidogenic, in that it has a longer lag phase for fibril formation and high ionic strength is frequently required (*13*, *15*). Ex vivo fibrils exhibit predominantly curved morphology (*18*, *19*), and they are presumably formed from the I_1 intermediate, or something similar. The formation of I_1 has also been observed in a series of mutants designed to destabilize each β-sheet of the native structure (*15*). Both the naturally occurring mutant N17D (*20*) and these designed mutants have higher populations of the I_1 intermediate (*15*, *20*). The resulting fibril morphology of the mutants depends on whether the mutation and conditions favor the I_1 or I_2 intermediate (*15*, *20*).

In this paper, we describe molecular dynamics (MD) simulations of β_2m in an investigation of unfolding to the amyloidogenic intermediate. We have performed simulations at both neutral and low pH to investigate pH-mediated conformational changes at physiological temperature (310 K) to approximate formation of amyloid in vivo (*18*, *19*). Our neutral-pH simulations serve as controls, and our low-pH conditions span a pH range of ∼2−4.2; Glu, Asp, and His residues are protonated, but the C-terminus is not. Consequently, our low-pH models should apply to both I_1 and I_2, which form sequentially with pH primarily affecting the relative populations of the intermediates. We have also performed 18 independent unfolding simulations at high temperature (498 K) and low pH to investigate later stages of the unfolding pathway and improve sampling. Here we propose all-atom structural models for I_1 and I_2 derived from these simulations.

In recent simulations of other amyloidogenic proteins at low pH, we observed the formation of α-sheet, which was first proposed by Pauling and Corey (*21*). α-Sheet is formed by hydrogen bonding between adjacent strands in the "α-extended chain" conformation, which is defined by an alternation of residues in the helical α_R and α_L conformations. This alternation yields an extended polypeptide chain, not α-helix. A notable feature of the α-sheet is the alignment of peptide NH groups on one side of the sheet and carbonyl groups on the other. In the β-sheet protein transthyretin, α-sheet formed over the strands that are highly protected in hydrogen exchange experiments probing amyloidogenic conditions (*22*). In lysozyme and the prion protein, α-sheets formed in the specific regions of the protein implicated in the amyloidogenic conversion (*21*). We have proposed that the formation of α-sheet may be a common conformational transition in the fibrillization of amyloidogenic proteins.

MATERIALS AND METHODS

Two different crystal structures were used as the starting conformations of β_2m in the MD simulations. The 1.5 Å crystal structure [PDB entry 1lds (*23*)] of the isolated monomer was used, and we denote this conformation A. The 1.9 Å crystal structure of β_2m bound to the MHC-1 molecule [PDB entry 1hsb (*24*)] was also used, and we denote this conformation B. MD simulations were performed at neutral pH (His neutral) and low pH (His protonated and charged, and Asp and Glu residues protonated and neutral). Lys and Arg residues were ionized in all simulations. The starting structures for all simulations were minimized 500 steps after applying the appropriate protonation state. Waters were added to make a box that extended at least 8 Å from any protein atom, resulting in the addition of approximately 4000 water molecules.

Simulations were performed at neutral and low pH at physiological temperature (310 K) for both the A and B conformers for 8 and 25 ns each, respectively. In addition, 498 K unfolding simulations were performed at low pH for 3 ns each, and our nomenclature for these simulations denotes the conformation of the starting structure (A or B) and the number of the trajectory for simplicity. Twelve independent unfolding simulations were performed at 498 K starting with the A (PDB entry 1lds) conformation, and we denote these A1−A12. Six independent thermal unfolding simulations at 498 K were performed starting with the B (PDB entry 1hsb) conformation, and we denote these B1−B6.

All simulations were performed with ENCAD(*25*). The protocols and the force field have been described previously (*26*, *27*), and the box volume was adjusted to give the experimental density: 0.992 g/mL at 310 K and 0.829 g/mL at 498 K (*28*). An 8 Å force-shifted cutoff was employed (*29*), and the nonbonded list was updated every two steps (every 4 fs). Our nonbonded cutoff routine effectively screens electrostatic interactions, thereby implicitly providing some ionic strength effects (*26*). Simulations were performed using the microcanonical ensemble and periodic boundary conditions. Structures were saved every 0.2 ps for analysis, resulting in 125 000 structures for the 25 ns trajectories and 15 000 structures for the 3 ns trajectories. All protein structure displays were created with PyMOL (*30*).

RESULTS

Conformational Properties of β_2m at 310 K. At 310 K, the C_α rms deviation from the crystal structure was greater at low pH than at neutral pH for both the A and B conformations (data not shown). The simulations at low pH had significantly larger rms deviations in the C−D and D−E loops compared with their behavior at neutral pH, although the rms fluctuations about the mean structure were similar. The regions of the sequence with the lowest C_α rmsd were the B-, C-, E-, and F-strands in simulations of both structures. The D-strand was the most dynamic element of well-defined secondary structure (Figure 1). Of the seven β-strands, the D-strand had the largest C_α rmsd and the largest rms fluctuations at both neutral and low pH.

The starting monomeric A conformation has more regular β-sheet structure and more β-sheet hydrogen bonding in the D-strand than the MHC-bound B conformation. The A conformer contained 69% repeating β-structure based on ϕ and ψ angles. The protein contained 44% β-structure, on average, in the neutral-pH simulations, but it maintained hydrogen bonding between the ABE and GFC strands. The

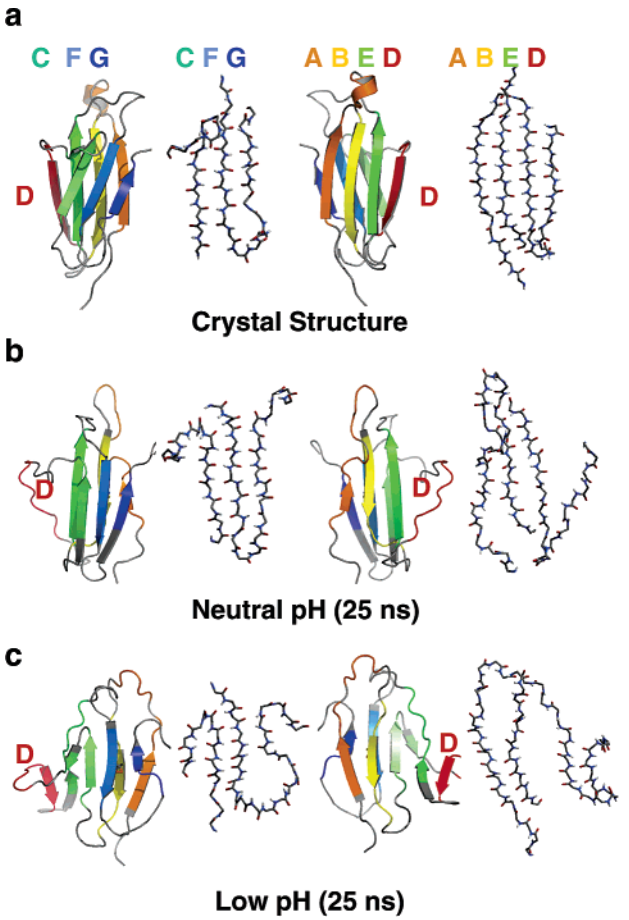

FIGURE 1: Simulations of β_2m at 310 K. (a) Crystal structure in ribbon and main chain modes for the CFG β-sheet and the ABED β-sheet. Residues 49−55 on the D-strand are colored red in the ribbon model. These residues exhibit NMR evidence of conformational exchange at neutral pH and increased backbone dynamics upon binding of Cu^{2+} (*13*). (b) Final 25 ns structure from the neutral pH simulation of the B conformation. Normal β-sheet structure is maintained over CFG- and ABE-strands. A standard β-bulge structure is formed over residues 91−94 of the F-strand and residues 65−68 of the E-strand. (c) Final 25 ns structure from the low-pH simulation of the B conformation. α-Sheet structure forms over residues 5−10 (A-strand), 24−28 (B-strand), 36−40 (C-strand), 42−45 (D′-strand), 53−56 (D-strand), 60−64 (E-strand), and 77−83 (F-strand).

loss of repeating β-sheet structure was localized to the D-strand, as well as transient and reversible fraying of the terminal A- and G-strands. We note that our definition for β-structure is based on ϕ and ψ angles, which are very sensitive and tend to underestimate β-content in structure that in fact forms β-sheet hydrogen bonds. In the simulation of the A conformation at 310 K and neutral pH, the D-strand became partially unstructured and adopted a conformation similar to that of the B conformer. Therefore, the D-strand is partially unstructured in neutral-pH simulations independent of the starting structure.

Experimentally, 28 residues are strongly protected from exchange with solvent in hydrogen exchange experiments at pH 7 (*11*). We can compare our 25 ns control simulation at neutral pH with these data; however, the comparison to hydrogen exchange data is necessarily indirect, as our simulations do not allow for the making and breaking of covalent bonds. Instead, we monitor the extent of interactions between the protein's amide hydrogens and solvent (*32*). If we require that an amide hydrogen interacts 10% of the total simulation time with solvent to exchange, then the neutral-pH simulation correctly predicts 17 of the 28 strongly protected amide hydrogens. The prediction improves to 23 of 28 if a 30% time cutoff is used.

The major difference between the simulations at low and neutral pH was the formation of α-sheet structure at low pH (Figure 1). Very little α-sheet hydrogen bonding was observed in the neutral-pH trajectory, although transient α-extended chain conformations were populated in the D-strand when it was not hydrogen bonded to the E-strand. In contrast, in the low-pH trajectories, α-sheet formed over the ABED and GFC sheets. The most persistent α-sheet hydrogen bonding formed between the A- and B-strands, the E- and D-strands, and the C- and G-strands. Some main chain hydrogen bonding was lost between the B- and E-strands late in the low-pH trajectory of the B conformer from 15 to 25 ns. Residues 43−46 in the C−D loop of the native conformation formed a nonnative α-sheet with residues 38−40 of the C-strand (Figure 1C). If this new strand D′ (in the loop between the C- and D-strands) extended, it could present a novel strand interface for self-assembly into amyloid, with a very nativelike topology (ABE and D′CFG). A similar strand extension (D′CFG) was observed in MD unfolding simulations of β_2m by Ma and Nussinov (*31*).

Thermal Unfolding at Low pH. β_2m lost most of its nativelike tertiary structure in 0.5−1 ns at high temperature such that the period of time from 1 to 3 ns represents acid-denatured conformations in all 18 unfolding simulations. To identify putative unfolding intermediates, we have used an all-versus-all C_α rmsd clustering of the structures (*33*−*35*). The distance between points in a three-dimensional (3D) reduced representation approximates the actual C_α rmsd between the structures. Thus, points that cluster in such a representation are necessarily similar and can be used to identify conformational ensembles and transitions between them (*35*). The majority of the most similar cross-peaks in the C_α rmsd comparison formed very early in the unfolding trajectories, from 0.1 to 0.5 ns (not shown). However, there were also such cross-peaks occurring late in the trajectories from 2 to 3 ns, where the conformations were significantly unfolded. Therefore, for each trajectory, we have identified the major early unfolding intermediate (I_1), which should correspond to the late nativelike intermediate observed experimentally in the folding direction. On a similar note, the late unfolding intermediates (I_2) should correspond to the early disordered intermediate observed experimentally in the folding direction. Examples of early unfolding intermediates (I_1) are shown in Figure 2, and the time periods over which the intermediates were populated are given in Table 1. The later intermediates were more difficult to pinpoint because of increased heterogeneity, so the entire 1−3 ns time period was used to represent the late unfolding intermediates.

There was considerable structural similarity between the 18 early unfolding intermediates (I_1). The majority of these intermediates retained nativelike tertiary structure in the B-, E-, F-, and C-strands, similar to the most stable regions of the protein in the simulations at 310 K. The I_1 intermediates were split into two classes, those that had nativelike tertiary structure and hydrogen bonding between the B- and E-strands and those that had nativelike tertiary structure and hydrogen

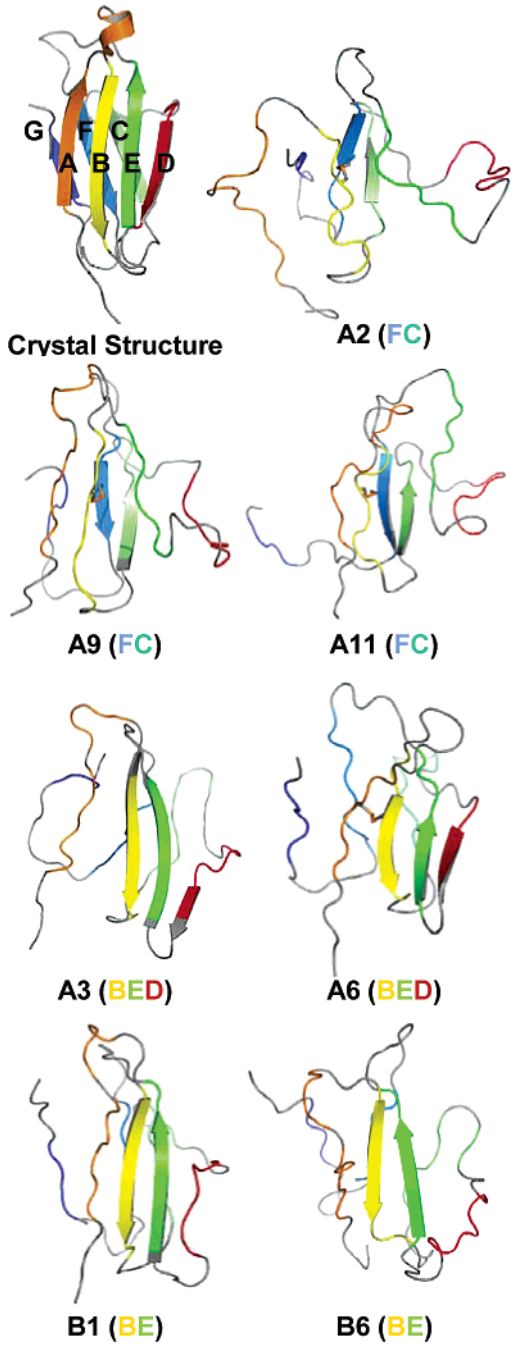

FIGURE 2: Representative early unfolding intermediates of β_2m. These intermediates were identified from 18 independent unfolding trajectories at 498 K. A crystal structure (PDB entry 1lds) is shown for comparison. Ribbons indicate the location of residual secondary structure. Residues 49−55 on the D-strand are colored red. Both β-sheets and α-sheets are shown with ribbons. Next to the intermediate name, the major elements of residual structure are denoted in parentheses.

bonding between the F- and C-strands. Of the 18 intermediates, 11 fell into the first category and seven in the latter. One intermediate (A7) fell into both categories. Another exception was the A10 intermediate, which had α-sheet structure over the E- and D-strands.

Comparison of the Early Unfolding Intermediate (I_1) with NMR Data. The conformational properties of the nativelike intermediate I_1 have been studied experimentally by equilibrium urea denaturation by monitoring the NH resonance intensity as a function of increasing urea concentration from

Table 1: Average Number of Protein Contacts in Nativelike I_1 Intermediates[a]

I_1 intermediate[b]	time period[c] (ps)	no. of native contacts	no. of total contacts	topology[d]
A1	155−205	131	192	BE
A2	240−475	136	216	FC
A3	110−230	173	245	BED
A4	205−360	149	221	FC
A5	175−330	131	192	ABE
A6	60−135	223	268	BED
A7	160−260	172	232	BE, FC
A8	270−405	126	194	FC
A9	165−280	168	239	FC
A10	315−420	130	218	ED
A11	75−180	196	243	FC
A12	165−300	166	229	BE
B1	135−210	201	253	BED
B2	140−275	155	227	AB, FC
B3	160−250	181	247	BE
B4	265−410	128	205	BE
B5	255−415	191	229	ABE
B6	195−305	169	239	BE

[a] Two residues were considered to be in contact if heavy atoms were within 4.6 Å of each other, or within 5.4 Å for pairs of aliphatic carbon atoms. The average numbers of native and total contacts are calculated for each time period that defines an intermediate. The native structure of the A and B conformation contains 337 and 349 contacts, respectively. [b] Name of the simulation intermediate or ensemble of intermediates. [c] Simulation time period defining the early unfolding intermediate. [d] Topology, or major strand interactions in the nativelike intermediates.

0 to 8 M with $^1H-^{15}N$ NMR (*36*). Under these solution conditions, this intermediate represents the dominant conformation, and the HN resonances of 11 residues are strongly resistant to urea denaturation at pH 3.6, with a midpoint of 4.5 M. To qualitatively compare our putative intermediate structures with this residue-specific experimental information, the number of intraprotein contacts made per residue was calculated for each trajectory, and in particular, the numbers of contacts in I_1 and I_2 were determined (Figure 3A). The regions with the largest changes in the number of contacts map to the residues with the largest midpoint of denaturation, the B-, E-, and F-strands (*36*) (Figure 3B). In the majority of the I_1 intermediates (15 of 18), the A- and G-strands were unstructured. In general, the intermediates with more extensive hydrogen bonding between the B- and E-stands had more native and total protein contacts than the intermediates with hydrogen bonding in the F- and C-strands (Table 1). When the 18 early intermediates are sorted by average number of total protein contacts, the top four intermediates all have residual structure in the B- and E-strands. Three of the top four intermediates have hydrogen bonding between the B-, E-, and D-strands, although in some cases it is through β-sheet and in others α-sheet. A greater number of molecules may unfold through an intermediate with residual structure in the BE-strands if they have more total protein contacts than intermediates with residual structure in the FC-strands. Therefore, MD-generated intermediates with residual structure in the BE-strands appear to be the most reasonable structural models to represent the experimental data for the I_1 intermediate (*36*). α-Sheet structure was observed in several of these intermediates over the BE- and BED-strands (Figure 3C). α-Sheet formation in these strands may also provide an additional explanation for the high resistance to urea denaturation for the B- and E-strands (Figure 4).

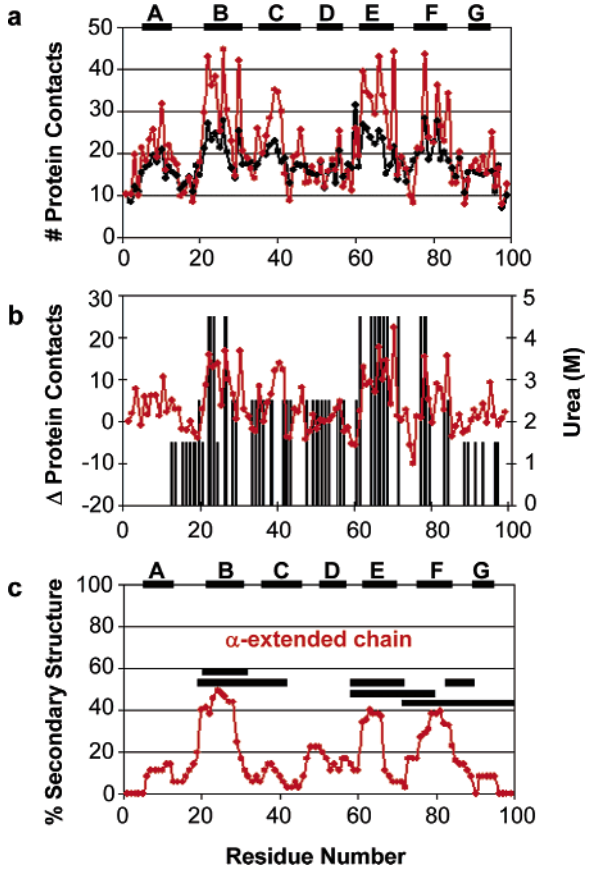

FIGURE 3: Properties of the unfolding intermediates. (a) The average number of contacts per residue in I_2 (colored black) compared to I_1 (colored red). (b) The difference between the average number of contacts per residue in I_1 and I_2 is shown as a red line. The midpoint of urea denaturation measured by $^1H-^{15}N$ NMR (*36*) is shown as a bar for each residue. The greatest change in contacts between I_1 and I_2 maps to the B- and E-strands, and these are more stable to urea. (c) Residual α-extended chain structure averaged over the entire ensemble of 18 independent unfolding trajectories. The percentage of time that there is persistent α-extended chain structure in the backbone is colored red. The requirement for persistence was that at least four residues had to exhibit the characteristic alternation between the α_R and α_L conformations, independent of the register. ϕ and ψ angles were required to be within ±30° of the following: 45° and 92° for α_R and −87° and −49° for α_L, respectively. Amyloidogenic peptides determined experimentally are shown as black bars (*38*−*43*).

Characterization of Disordered Intermediate I_2. While the 18 early unfolding intermediates (I_1) were similar by C_α rmsd (7.3 ± 1.6 Å) and remained roughly nativelike, the late intermediates (I_2) were more varied, but some were similar in overall shape and topology. Nine of the late intermediates adopted an elongated loop structure, with the disulfide and the terminal strands at one end and the residues comprising the D-strand at the other (Figure 4). The disulfide added a significant restraint to the unfolded conformations, thereby contributing to the gross similarity of these late intermediates. Given the difficulty in precisely clustering these conformations, the 1−3 ns time period of the 18 trajectories was pooled to create a 36 ns (180 000 structures) ensemble for the late unfolding intermediate. Figure 3A shows the average number of contacts formed per residue in this ensemble. The greatest number of hydrophobic contacts was in regions defined by residues 22−41, 62−70, and 78−84. Figure 3C shows the ensemble average of residual α-extended chain

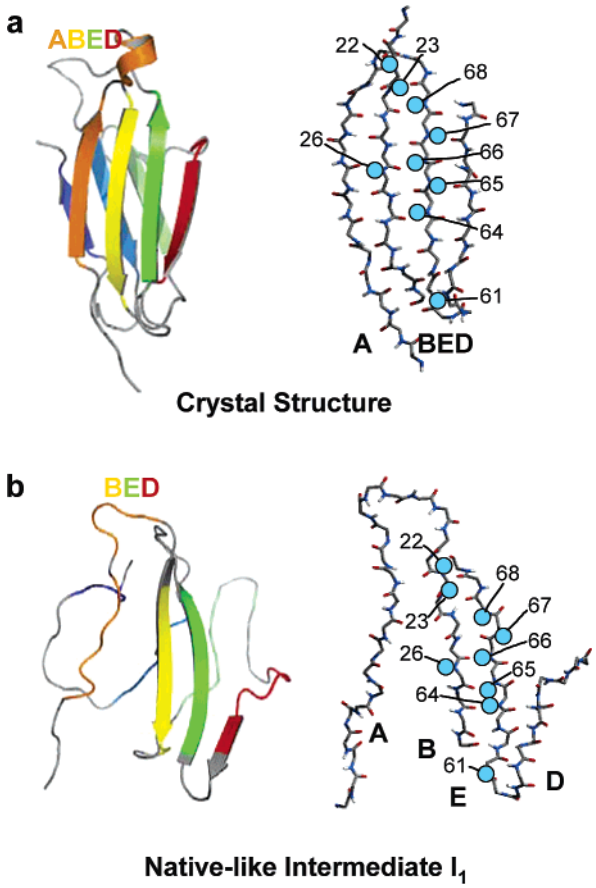

FIGURE 4: Nativelike intermediate (I_1) with α-sheet structure over the BED-strands. (a) The residues with the greatest stability to urea denaturation at pH 3.6 are highlighted with blue circles on the monomeric crystal structure (PDB entry 1lds) (*36*). (b) These same amides shown on a representative I_1 α-sheet structure, A3. A single peptide plane flip of the amide plane of residue 67 leads to a continuous α-sheet structure from residue 62 to 68.

structure, exhibiting the characteristic alternation of α_R and α_L conformations. The greatest consensus across the I_2 intermediates was the proximity of extended conformations for residues 26−40, particularly the B-strand, and residues 59−79, comprising the E- and F-strands and the intervening residues, which we denote F′ (Figure 5). A large population of residual α-extended chain conformation was observed in the region of residues 17−30 and 70−82, even though the structure was very disrupted. There was also significant hydrophobic clustering of side chains between these two regions, which contributed to the stability of the elongated intermediates.

DISCUSSION

The Native State of β_2m Is Highly Dynamic. At 310 K, the larger C_α rmsd of the low-pH simulation compared with that at neutral pH was expected, as pH perturbation alone (below pH 4.7) is sufficient for the formation of the nativelike partially unfolded state (I_1) (*13*). The regions of the sequence with the lowest C_α rmsd were comprised of the B-, C-, E-, and F-strands, which are thought to remain partially structured in the nativelike I_1 intermediate (*11*, *37*). The D-strand had the largest C_α rmsd and the largest rms fluctuations at both neutral and low pH. In neutral-pH simulations of both the A and B conformers, the D-strand was very dynamic with significant fluctuations from the native conformation.

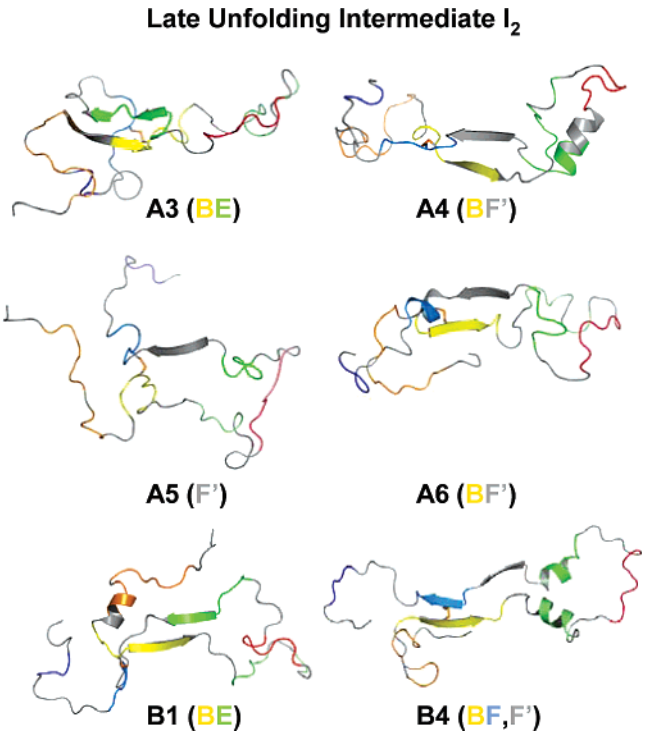

FIGURE 5: Representative late unfolding intermediates (I_2) of β_2m. These intermediates were identified from 18 independent unfolding trajectories at 498 K. Segments of residual α-helical structure and α-extended chain structure are shown as ribbons. Residues 49−55 on the D-strand are colored red.

The conformation of the D-strand is the most significant difference between the crystal structures of the monomeric (*23*) and MHC-1-bound forms (*24*). The largest region of rms deviation between the NMR structure (*37*) (pH 6.6) and MHC-1-bound crystal structure is for the C−D loop, D-strand, and D−E loop (residues 41−48 and 56−62). The D-strand appears to undergo slight rearrangement upon binding with the MHC-1 molecule and to be partially disordered in the monomer structure. NMR data for the monomer at pH 6.6 and 310 K reflect structural dispersion over residues 53, 54, and 57−61, consistent with conformational exchange along the D-strand, as well as unstable hydrogen bonding between the D- and E-strands (*37*).

In the absence of Cu^{2+} at pH 7, the D-strand is the least protected β-strand in hydrogen exchange experiments, even compared to some amides on the terminal A- and G-strands (*11*). We have compared our 25 ns control simulation at neutral pH with the experimental hydrogen exchange data at pH 7. Our simulation results are in good agreement with the experimental observation that the D-strand has the lowest protection factors of any of the strands. On average, the amide hydrogens of residues 49−55 on the D-strand interacted with solvent 75% of the simulation time, compared with 3% for residue 8 on the N-terminal A-strand, and 0−2% for residues 91, 92, and 95 on the C-terminal G-strand.

There is also NMR evidence for increased backbone dynamics in the D-strand upon binding of Cu^{2+} at pH 7 (*11*). Three of four histidine residues (His13, His31, and His51) are involved in Cu^{2+} binding at pH 7, while only two of these residues (His13 and His31) are involved in Cu^{2+} binding at pH 6.5. $^1H-^{15}N$ HSQC spectra recorded at pH 6.2, 6.5, and 7.0 show a pH-dependent peak shift for only His51, indicating that His51 is deprotonated and capable of binding Cu^{2+} in the pH range of 6.5−7.0. This observation is consistent with thermal denaturation studies of β_2m in the presence and absence of Cu^{2+}, which indicate that β_2m is more destabilized by binding of Cu^{2+} at pH 7 than at pH 6.5. β_2m presumably has a higher affinity for Cu^{2+} at pH 7 due to the change in the binding site.

During the titration with Cu^{2+}, steady state $^1H-^{15}N$ heteronuclear NOEs were used to monitor restricted backbone motions on the picosecond to nanosecond time scale after considering the paramagnetic contribution of the Cu^{2+} ion. Of the three residues involved in Cu^{2+} binding at pH 7, the residues near His51 (residues 49−55) showed the largest increase in backbone dynamics. The authors suggested that this specific effect on protein dynamics may be because His13 and His31 are located at the end of a β-strand and in a loop, respectively, whereas His51 is in the center of a solvent-exposed β-strand. The authors conclude that the D-strand (residues 49−55) becomes more dynamic upon binding of Cu^{2+} at pH 7. This partial unfolding of the D-strand may contribute to the population of nativelike intermediate I_1, and the accumulation of fibrils under physiological conditions. Even in the absence of Cu^{2+} at pH 7, the D-strand was the least protected β-strand in hydrogen exchange experiments, suggesting conformational exchange in the neutral-pH native state. Therefore, our MD results are in agreement with the NMR evidence for structural heterogeneity of the D-strand.

The Nativelike Intermediate (I_1) at Low pH. The majority of the identified I_1 unfolding intermediates retained nativelike tertiary structure in the B-, C-, E-, and F-strands, similar to the most stable regions of the protein in the 310 K, neutral-pH simulations. The I_1 intermediates were split into two classes, those with nativelike tertiary structure and hydrogen bonding between the B- and E-strands and those with retention of structure between the F- and C-strands (the 310 K, low-pH simulations fell into this category). The BE intermediates were more populated in unfolding trajectories and had a larger number of total protein contacts than the FC intermediates. The extent of tertiary structure in I_1 is consistent with the results from equilibrium urea denaturation experiments (*36*). The B- and E-strands exhibited the largest difference in the number of contacts by MD between I_1 and I_2, as well as the greatest stability against urea denaturation at pH 3.5 (*36*), suggesting that the I_1 intermediate at pH 3.6 has residual structure in the B- and E-strands. The B-, C-, E-, and F-strands have been mapped to amyloidogenic peptides (*38*−*43*); however, only the B- and E-strands have been mapped to minimal peptides spanning just a single β-strand. A peptide spanning both the B- and C-strands (residues 20−41) is amyloidogenic (*39*, *40*), as well as a peptide derived from only the B-strand (residues 20−31) (*41*). A peptide spanning the E- and F-strands (residues 59−79) is also amyloidogenic (*38*). These amyloidogenic sequences map to the regions of high α-sheet structure content (Figure 3B). In nativelike unfolding intermediates with a BED-strand topology, α-sheet structure exhibits a left-handed twist like normal β-sheets. Previous three-stranded α-sheet structures observed in similar simulations of transthyretin were very flat, rarely with more than a 2° rotation between strands (*21*, *22*). It is possible that the twisted α-sheet structure over the BED-strand contributes to the curved fibril morphology.

Disordered Intermediate (I_2) at Low pH. Several of the late intermediates contained an elongated loop structure, with the disulfide and the terminal strands at one end and the residues comprising the D-strand at the other (Figure 4A). The intact disulfide bond is necessary for fibrillization (*44*−*46*). Consistent with the need for some structure in amyloidogenic precursors, transthyretin only forms amyloid fibrils from the nativelike intermediate, not its acid-induced denatured state or molten globule state, but its unfolded state is presumably less structured due to the absence of disulfide bonds (*47*). Many of the MD-generated late intermediates of β_2m had nonnative helical structure in different positions along the sequence: there was a greater than average helical content over strands B−F. This observation is in agreement with chemical shift deviations of the denatured state at pH 2.5 measured by heteronuclear NMR (*45*). In particular, the C- and E-strands display the greatest helical content by both MD and NMR, as measured by chemical shift deviations for $^{13}C_\alpha$ and ^{13}CO and by $^3J_{NH\alpha}$ coupling constants ($^3J_{NH\alpha}$ < 4 Hz) (*45*).

Ma and Nussinov (*31*) also observed nonnative helical structure in their MD simulations of β_2m, and they argue that amyloidogenesis proceeds via $\beta-\alpha-\beta$ transitions. In contrast, both the MD simulations presented here, and similar work on disease-associated variants of lysozyme (manuscript in preparation), suggest that helical structure does not directly nucleate amyloid fibrils. It is more likely that amyloid forms from extended conformations, β-strand conformations, poly(proline) II structure, and α-extended chain. Instead, transient formation of helix is more likely to be protective against amyloid formation.

The greatest similarity between the late intermediates (I_2) was the proximity of extended conformations for residues 26−40, comprising the B- and C-strands, and residues 59−79, comprising the E- and F-strands (Figure 4). The largest population of residual α-extended chain conformations also corresponded to these regions. Interestingly, these regions of the sequence exhibit higher propensities for amyloid formation than other regions of the sequence (Figure 3C) (*38*−*43*). The greatest number of hydrophobic contacts in the late unfolding intermediate was in residues 22−41, 62−70, and 78−84. These observations are in qualitative agreement with recent ^{15}N transverse relaxation experiments on the unfolded state of β_2m at pH 2.5 (*17*), which provide evidence for two persistent hydrophobic clusters involving residues 29−51 and 57−79.

Proposed Mechanism for Self-Assembly. We have proposed that as an amyloidogenic protein unfolds under mildly acidic conditions, α-sheet facilitates self-association into amyloid protofibrils (*21*, *22*). According to a dipole assembly model (*48*), proteins build up a molecular dipole upon encountering low-pH conditions. We postulate that as the molecular dipole builds, individual peptide groups undergo peptide plane flips and become aligned with the overall molecular dipole to form an α-sheet. Partial charges from the α-sheet polypeptide backbone create two complementary charged interfaces for self-assembly. Once the soluble protofibrils are formed via an α-sheet intermediate, the transition from α-sheet to β-sheet may become increasingly more favorable as the protofibrils move from the cytotoxic soluble phase to the insoluble more highly ordered amyloid fibrils (*21*).

Our low-pH results at 310 K show that β_2m can form α-sheet in the A−F-strands, and therefore, self-assembly through an α-sheet intermediate may be possible in a very nativelike topology (Figure 6A). However, two distinct partially unfolded intermediates have been implicated by experiment to be the precursors to different fibril morphologies (*15*). We propose that α-sheet and α-extended chain structures facilitate self-assembly in these two partially unfolded prefibrillar amyloidogenic intermediates (Figure 6A,B). In our unfolding simulations, I_1 was very nativelike with hydrogen-bonded α-sheet structure in the B- and E-strands. The late unfolding intermediate was significantly more disordered, but maintained an extended elongated structure, with the proximity of the B- and F-strands due to the constraint of the disulfide. Even though the late unfolding intermediate was very disordered, it retained residual α-extended chain backbone configurations in the B- and F-strands, which have both been mapped as amyloidogenic peptides (*38*−*43*). We propose that amyloid formation occurs in the late intermediate through residual α-extended chain conformations in these highly disordered states, possibly through an intermolecular α-sheet involving regions of α-extended chain (for example, residues 17−40 and 59−82) (Figure 6C).

Since many non-disease-related proteins form fibrils under extreme conditions, it has been proposed that essentially any sequence can form amyloid (*49*). However, there is also evidence for sequence preferences for amyloid formation, and a number of studies investigating peptides of β_2m have shown that some of these peptides are amyloidogenic while others are not, at least under the conditions that were investigated. In a systematic peptide scanning study probing the seven β-strands, only two peptides were amyloidogenic, both of which cover the E-strand (residues 59−71 and 59−79) (*38*). Another study found two amyloidogenic peptides (residues 20−41 and 20−31), both containing residues from the B-strand (*39*−*41*). Also, a peptide spanning the C-terminal F- and G-strands (residues 72−99) is amyloidogenic (*42*), as well as a shorter peptide in this region (residues 83−89) (*43*). Residues 83−89 are different in the human and mouse proteins, and interestingly, the human protein forms amyloid while the mouse protein does not (*43*). When the human residues are engineered into the mouse protein, it then forms amyloid (*42*). Thus, there are specific sequence preferences to amyloid formation in β_2m. It has been proposed that segments corresponding to amyloidogenic peptides may contribute to the nucleation of protein−protein interactions during aggregation (*38*, *40*, *42*). In the regard, it is interesting to note that there are similarities between the B-, E-, and F-strands: they have the greatest number of protein contacts in both I_1 and I_2, and they contain residual α-extended chain structure.

Full-length β_2m fibrils yield strong 4.8 Å meridional and 11.7 Å equatorial reflections by X-ray fiber diffraction (*43*). A two-stranded β-sheet was the best fit to the data as the repeat for the β_2m fibril (*35*). On the basis of these results, Ivanova and co-workers proposed a model in which the core of the fibril is formed by the F- and G-strands (*43*). In the MD-generated I_1 intermediates, the F-strand was mostly disordered and did not form a hairpin with the G-strand. The hairpin was not present in the late intermediates either. Nevertheless, both the G- and F-strands exhibited residual α-extended chain conformations in I_2, which may explain

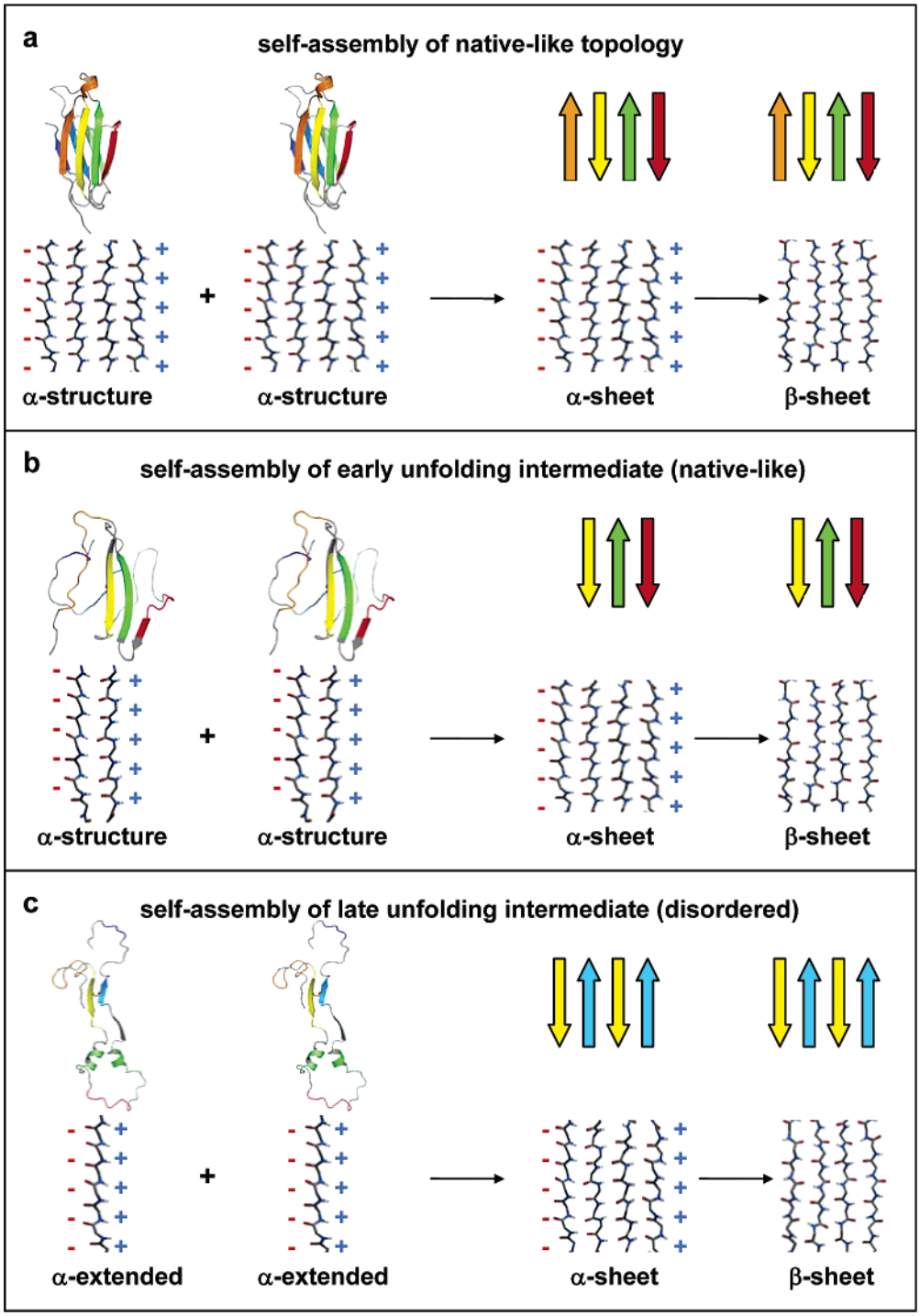

FIGURE 6: Proposed mechanism for self-assembly for β_2m through an α-sheet intermediate. (a) As α-sheet forms extensively at low pH in the native topology, fibrils may form through an intermediate with a native or nativelike topology (CFG, ABED or D′CFG, ABE). (b) The I_1 intermediate may form intermolecular interactions through persistent α-sheet structure. An example with residual structure in the B- and E-strands is provided. (c) The I_2 intermediate may form intermolecular α-sheet interactions through persistent α-extended chain structure in the disordered state. Significant structural rearrangement may occur after the formation of the initial intermolecular interactions.

why they together form an amyloidogenic peptide (*42*), perhaps via intermolecular interactions rather than formation of an intramolecular hairpin. The G-strand alone is not amyloidogenic (*38*). Our model for the self-assembly of both I_1 and I_2 (Figure 5) is in reasonable agreement with the interpretation of the X-ray fiber diffraction pattern, namely, that a two-stranded sheet is the most likely core repeat for the β_2m fibril (*43*). We propose that I_1 forms fibrils primarily via the B- and E-strands (or BED-strands) and that I_2 forms fibrils primarily through the B- and F-strands. The B-, E-, and F-strands have all been mapped to amyloidogenic peptides (*38*−*43*). Although most late intermediates did not exhibit direct α-sheet hydrogen bonding between the B- and F-strands, it did occur. The topology of this intermediate was unexpected, and demonstrates that hydrogen bonding between the B- and F-strands is possible in the denatured state, even though these strands are on opposite sides of the native β-sandwich.

Our proposed model for self-assembly is also consistent with proteolysis and hydrogen exchange experiments of β_2m

fibrils. Full-length β_2m is the most common component of ex vivo fibrils; however, up to 30% of the protein in the fibrils is composed of two truncated forms resulting from cleavage at residues 6 and 19 (*50*). Fibrils grown in vitro can also be proteolyzed at residues 87, 91, 96, and 98, leaving an intact protease-resistant core comprised of residues 20−87 (*51*). This finding suggests that the A- and G-strands are not incorporated into the mature fibrils. A hydrogen exchange study of β_2m fibrils is in agreement with this observation: these are the only strands not significantly protected in fibrils (*52*). However, additional hydrogen exchange studies of β_2m fibrils indicate that the G-strand is sometimes protected from exchange, and therefore may be incorporated (*53*). These studies reveal a large degree of heterogeneity and that specific residues in the polypeptide chain are not always in the same chemical environment (*53*). This heterogeneity within amyloid fibrils of the same morphology is unexpected from the conventional view of β-sheet self-assembly. An α-sheet intermediate model may explain the heterogeneity. The initial self-assembly interface may be more specific for the backbone, and the spatial requirements for α-sheet hydrogen bonds are not as strict as for formation of β-structure; i.e., alternate registers are more easily accommodated. Therefore, an α-sheet mechanism for self-assembly may explain how building blocks of slightly different topologies add to the same protofibril and contribute to heterogeneous chemical environments for individual residues in the polypeptide chain.

REFERENCES

1. Maenaka, K., and Jones, E. Y. (1999) MHC superfamily structure and the immune system, *Curr. Opin. Struct. Biol. 9*, 745−753.
2. Floege, J., and Ehlerding, G. (1996) β-2-Microglogulin-associated amyloidosis, *Nephron 72*, 9−26.
3. Floege, J., and Ketteler, M. (2001) β2-Microglobulin-derived amyloidosis: An update, *Kidney Int. 59*, 164−171.
4. Pepys, M. B. (1995) Amyloidosis, in *Oxford Textbook of Medicine* (Weatherall, D. J., Ledingham, J. G., and Warrel, D. A., Eds.) 3rd ed., pp1512−1524, Oxford University Press, Oxford, U.K.
5. Lucchi, L., Fiore, G. B., Guadagni, G., Perrone, S., Malaguti, V., Caruso, F., Fumero, R., and Albertazzi, A. (2004) Clinical evaluation of internal hemodiafiltration (iHDF): A diffusive-convective technique performed with internal filtration enhanced high-flux dialyzers, *Int. J. Artif. Organs 27*, 414−419.
6. Zaoui, P. M., Stone, W. J., and Hakim, R. M. (1990) Effects of dialysis membranes on β2-microglobulin production and cellular expression, *Kidney Int. 38*, 962−968.
7. Okon, M., Bray, P., and Vucelic, D. (1992) ^{1}H NMR assignments and secondary structure of human β2-microglobulin in solution, *Biochemistry 31*, 8906−8915.
8. Morgan, C. J., Gelfand, M., Atreya, C., and Miranker, A. D. (2001) Kidney dialysis-associated amyloidosis: A molecular role for copper in fiber formation, *J. Mol. Biol. 309*, 339−345.
9. Chiti, F., De Lorenzi, E., Grossi, S., Mangione, P., Giorgetti, S., Caccialanza, G., Dobson, C. M., Ramponi, G., and Bellotti, V. (2001) A partially structured species of β2-microglobulin is significantly populated under physiological conditions and involved in fibrillogenesis, *J. Biol. Chem. 276*, 46714−46721.
10. Eakin, C. M., Knight, J. D., Morgan, C. J., Gelfand, M. A., and Miranker, A. D. (2002) Formation of a copper specific binding site in non-native states of β-2-microglobulin, *Biochemistry 41*, 10646−10656.
11. Villanueva, J., Hoshino, M., Katou, H., Kardos, J., Hasegawa, K., Naiki, H., and Goto, Y. (2004) Increase in the conformational flexibility of β2-microglobulin upon copper binding: A possible role for copper in dialysis-related amyloidosis, *Protein Sci. 13*, 797−809.
12. Eakin, C. M., Attenello, F. J., Morgan, C. J., and Miranker, A. D. (2004) Oligomeric assembly of native-like precursors precedes amyloid formation by β-2-microglobulin, *Biochemistry 43*, 7808−7815.
13. McParland, V. J., Kad, N. M., Kalverda, A. P., Brown, A., Kirwin-Jones, P., Hunter, M. G., Sunde, M., and Radford, S. E. (2000) Partially unfolded states of β_2-microglobulin and amyloid formation in vitro, *Biochemistry 39*, 8735−8746.
14. Chiti, F., Mangione, P., Andreola, A., Giorgetti, S., Stefani, M., Dobson, C. M., Bellotti, V., and Taddei, N. (2001) Detection of two partially structured species in the folding process of the amyloidogenic protein β2-microglobulin, *J. Mol. Biol. 307*, 379−391.
15. Smith, D. P., Jones, S., Serpell, L. C., Sunde, M., and Radford, S. E. (2003) A systematic investigation into the effects of protein destabilization on β2-microglobulin amyloid formation, *J. Mol. Biol. 330*, 943−954.
16. Gosal, W. S., Morten, I. J., Hewitt, E. W., Smith, D. A., Thomson, N. H., and Radford, S. E. (2005) Competing pathways determine fibril morphology in the self-assembly of β_2-microglobulin into amyloid, *J. Mol. Biol.* (in press).
17. Platt, G. W., McParland, V. J., Kalverda, A. P., Homans, S. W., and Radford, S. E. (2005) Dynamics in the unfolded state of β2-microglobulin studied by NMR, *J. Mol. Biol. 346*, 279−294.
18. Inoue, S., Kuroiwa, M., Ohashi, K., Hara, M., and Kisilevsky, R. (1997) Ultrastructural organization of hemodialysis-associated β2-microglobulin amyloid fibrils, *Kidney Int. 52*, 1543−1549.
19. Nishi, S., Ogino, S., Maruyama, Y., Honma, N., Gejyo, F., Morita, T., and Arakawa, M. (1990) Electron-microscopic and immunohistochemical study of β-2-microglobulin-related amyloidosis, *Nephron 56*, 357−363.
20. Kad, N. M., Thomson, N. H., Smith, D. P., Smith, D. A., and Radford, S. E. (2001) β_2-Microglobulin and its deamidated variant, N17D form amyloid fibrils with a range of morphologies in vitro, *J. Mol. Biol. 313*, 559−571.
21. Armen, R. S., DeMarco, M. L., Alonso, D. O. V., and Daggett, V. (2004) Pauling and Corey's α-pleated sheet structure may define the prefibrillar amyloidogenic intermediate in amyloid disease, *Proc. Natl. Acad. Sci. U.S.A. 101*, 11622−11627.
22. Armen, R. S., Alonso, D. O. V., and Daggett, V. (2004) Anatomy of an amyloidogenic intermediate: Conversion of β-sheet to α-sheet structure in transthyretin at acidic pH, *Structure 12*, 1847−1863.
23. Trinh, C. H., Smith, D. P., Kalverda, A. P., Phillips, S. E. V., and Radford, S. E. (2004) Crystal structure of monomeric human β-2-microglobulin reveals clues to its amyloidogenic properties. *Proc. Natl. Acad. Sci. U.S.A. 96*, 9771−9776.
24. Guo, H. C., Jardetzky, T. S., Garrett, T. P., Lane, W. S., Strominger, J. L., and Wiley, D. C. (1992) Different length peptides bind to HLA-Aw68 similarly at their ends but bulge out in the middle, *Nature 360*, 364−366.
25. Levitt, M. (1990) *ENCAD: Energy Calculations and Dynamics*, Stanford University, Palo Alto, CA, and Yeda, Rehovot, Israel.
26. Levitt, M., Hirshberg, M., Sharon, R., and Daggett, V. (1995) Potential energy function and parameters for simulations of the molecular dynamics of proteins and nucleic acids in solution, *Comput. Phys. Commun. 91*, 215−231.
27. Levitt, M., Hirshberg, M., Sharon, R., Laidig, K. E., and Daggett, V. (1997) Calibration and testing of a water model for simulation of the molecular dynamics of proteins and nucleic acids in solution, *J. Phys. Chem. B 101*, 5051−5061.
28. Kell, G. S. J. (1967) Precise representation of volume properties of water at one atmosphere. *Chem. Eng. Data 12*, 66−69.
29. Beck, D. A., Armen, R. S., and Daggett, V. (2005) Cutoff size need not strongly influence molecular dynamics results for solvated polypeptides, *Biochemistry 44*, 609−616.
30. DeLano, W. L. (2002) *The PyMOL Molecular Graphics System*, DeLano Scientific, San Carlos, CA.
31. Ma, B., and Nussinov, R. (2003) Molecular dynamics simulations of the unfolding of β_2-microglobulin and its variants, *Protein Eng. 16*, 561−575.
32. Alonso, D. O. V., and Daggett, V. (1995) Molecular dynamics simulations of protein unfolding and limited refolding: Characterization of partially unfolded states of ubiquitin in 60% methanol and in water, *J. Mol. Biol. 247*, 501−520.
33. Li, A. J., and Daggett, V. (1994) Characterization of the transition state of protein unfolding by use of molecular dynamics: Chymotrypsin inhibitor 2, *Proc. Natl. Acad. Sci. U.S.A. 91*, 10430−10434.
34. Li, A. J., and Daggett, V. (1998) Molecular dynamics simulation of the unfolding of barnase: Characterization of the major intermediate, *J. Mol. Biol. 275*, 677−694.

35. Jemth, P., Gianni, S., Day, R., Li, B., Johnson, C. M., Daggett, V., and Fersht, A. R. (2004) Demonstration of a low-energy on-pathway intermediate in a fast-folding protein by kinetics, protein engineering, and simulation, *Proc. Natl. Acad. Sci. U.S.A. 101*, 6450−6455.
36. McParland, V. J., Kalverda, A. P., Homans, S. W., and Radford, S. E. (2002) *Nat. Struct. Biol. 9*, 326−331.
37. Verdone, G., Corazza, A., Viglino, P., Pettirossi, F., Giorgetti, S., Mangione, P., Andreola, A., Stoppini, M., Bellotti, V., and Esposito, G. (2002) The solution structure of human β2-microglobulin reveals the prodromes of its amyloid transition, *Protein Sci. 11*, 487−499.
38. Jones, S., Manning, J., Kad, N. M., and Radford, S. E. (2003) Amyloid-forming peptides from β2-microglobulin: Insights into the mechanism of fibril formation in vitro, *J. Mol. Biol. 325*, 249−257.
39. Kozhukh, G. V., Hagihara, Y., Kawakami, T., Hasegawa, K., Naiki, H., and Goto, Y. (2002) The intrastrand disulfide bond of β_2-microglobulin is not essential for the immunoglobulin fold at neutral pH, but is essential for amyloid fibril formation at acidic pH, *J. Biol. Chem. 277*, 1310−1315.
40. Ohhashi, Y., Hasegawa, K., Naiki, H., and Goto, Y. (2004) Optimum amyloid fibril formation of a peptide fragment suggests the amyloidogenic preference of β2-microglobulin under physiological conditions, *J. Biol. Chem. 279*, 10814−10821.
41. Hiramatsu, H., Goto, Y., Naiki, H., and Kitagawa, T. (2004) Core structure of amyloid fibril proposed from IR-microscope linear dichroism, *J. Am. Chem. Soc. 126*, 3008−3009.
42. Ivanova, M. I., Gingery, M., Whitson, L. J., and Eisenberg, D. (2003) Role of the C-terminal 28 residues of β2-microglobulin in amyloid fibril formation, *Biochemistry 42*, 13536−13540.
43. Ivanova, M. I., Sawaya, M. R., Gingery, M., Attinger, A., and Eisenberg, D. (2004) An amyloid-forming segment of β2-microglobulin suggests a molecular model for the fibril, *Proc. Natl. Acad. Sci. U.S.A. 101*, 10584−10589.
44. Smith, D. P., and Radford, S. E. (2001) Role of the single disulphide bond of β_2-microglobulin in amyloidosis in vitro, *Protein Sci. 10*, 1775−1784.
45. Katou, H., Kanno, T., Hoshino, M., Hagihara, Y., Tanaka, H., Kawai, T., Hasegawa, K., Naiki, H., and Goto, Y. (2002) The role of disulfide bond in the amyloidogenic state of β_2-microglobulin studied by heteronuclear NMR, *Protein Sci. 11*, 2218−2229.
46. Hong, D. P., Gozu, M., Hasegawa, K., Naiki, H., and Goto, Y. (2002) Conformation of β2-microglobulin amyloid fibrils analyzed by reduction of the disulfide bond, *J. Biol. Chem. 277*, 21554−21560.
47. Kelly, J. W., Colon, W., Lai, Z., Lashuel, H., McCulloch, J., McCutchen, S., Miroy, G. J., and Peterson, S. A. (1997) Transthyretin quaternary and tertiary structural changes facilitate misassembly into amyloid, *Adv. Protein Chem. 50*, 161−181.
48. Xu, S. H., Bevis, B., and Arnsdorf, M. F. (2001) The assembly of amyloidogenic yeast sup35 as assessed by scanning (atomic) force microscopy: An analogy to linear colloidal aggregation? *Biophys. J. 81*, 446−456.
49. Chiti, F., Webster, P., Taddei, N., Clark, A., Stefani, M., Ramponi, G., and Dobson, C. M. (1999) Designing conditions for in vitro formation of amyloid protofilaments and fibrils, *Proc. Natl. Acad. Sci. U.S.A. 96*, 3590−3594.
50. Stoppini, M., Arcidiaco, P., Mangione, P., Giorgetti, S., Brancaccio, D., and Bellotti, V. (2000) Detection of fragments of β2-microglobulin in amyloid fibrils, *Kidney Int. 57*, 349−350.
51. Monti, M., Principe, S., Giorgetti, S., Mangione, P., Merlini, G., Clark, A., Bellotti, V., Amoresano, A., and Pucci, P. (2002) Topological investigation of amyloid fibrils obtained from β2-microglobulin, *Protein Sci. 11*, 2262−2369.
52. Hoshino, M., Katou, H., Hagihara, Y., Hasegawa, K., Naiki, H., and Goto, Y. (2002) Mapping the core of the β_2-microglobulin amyloid fibril by H/D exchange, *Nat. Struct. Biol. 9*, 332−336.
53. Yamaguchi, K., Katou, H., Hoshino, M., Hasegawa, K., Naiki, H., and Goto, Y. (2004) Core and heterogeneity of β2-microglobulin amyloid fibrils as revealed by H/D exchange, *J. Mol. Biol. 338*, 559−571.

BI050731H